ADVANCED MATERIALS

[9] X. He, M. Trudeau, D. M. Antonelli, *Adv. Mater.* **2000**, *12*, 1036.
[10] S. Murray, M. Trudeau, D. M. Antonelli, *Adv. Mater.* **2000**, *12*, 1339.
[11] B. Ye, M. Trudeau, D. M. Antonelli, *Adv. Mater.* **2001**, *13*, 29.
[12] B. Ye, M. Trudeau, D. M. Antonelli, *Adv. Mater.* **2001**, *13*, 561.
[13] M. Vettraino, B. Ye, X. He, D. M. Antonelli, *Aust. J. Chem.* **2001**, *54*, 85.
[14] M. Vettraino, X. He, M. Trudeau, J. E. Drake, D. M. Antonelli, *Adv. Funct. Mater.* **2002**, *12*, 174.
[15] a) D. J. Kim, M. H. Lee, D. Y. Lee, J. S. Han, *J. Biomed. Mater. Res.* **2000**, *53*, 438. b) K. A. Gross, L. Berzina, R. Cimdins, V. Gross, *Ceram. Int.* **1999**, *25*, 231.
[16] a) B. Tian, X. Liu, B. Tu, C. Z. Yu, J. Fan, L. Wang, S. Xie, G. D. Stucky, D. Zhao, *Nat. Mater.* **2003**, *2*, 159. b) B. Tian, H. Yang, X. Liu, S. Xie, C. Yu, J. Fan, B. Tu, D. Zhao, *Chem. Commun.* **2002**, 1824.
[17] X. Chen, R. Ferrigno, J. Yang, G. A. Whitesides, *Langmuir* **2002**, *18*, 7009.
[18] S. Haymond, G. T. Babcock, G. M. Swain, *J. Am. Chem. Soc.* **2002**, *124*, 10 634.
[19] a) A. S. Haas, D. L. Pilloud, K. S. Reddy, G. T. Babcock, C. C. Moser, J. K. Blasie, P. L. Dutton, *J. Phys. Chem. B* **2001**, *105*, 11 351. b) A. Avila, B. W. Gregory, K. Niki, T. M. Cotton, *J. Phys. Chem. B* **2000**, *104*, 2759.
[20] T. Ferri, A. Poscia, F. Ascoli, R. Santucci, *Biochim. Biophys. Acta* **1996**, *1298*, 102.
[21] E. Laviron, *J. Electroanal. Chem.* **1979**, *101*, 19.
[22] A. El Kasmi, M. C. Leopold, R. Galligan, R. T. Robertson, S. S. Saavedra, K. El Kacemi, E. F. Bowden, *Electrochem. Commun.* **2002**, *4*, 177.
[23] H. Ju, S. Liu, B. Ge, F. Lisdat, F. W. Scheller, *Electroanalysis* **2002**, *14*, 141.

Permeable, Microporous Polymeric Membrane Materials Constructed from Discrete Molecular Squares**

By *Melinda H. Keefe*, *Jodi L. O'Donnell*, *Ryan C. Bailey*, *SonBinh T. Nguyen*, and *Joseph T. Hupp**

Molecular squares, triangles, rectangles, and related structures, consisting of transition-metal corners and difunctional ligand edges, are the synthetic focus of a substantial segment of contemporary coordination chemistry.[1–4] The attraction of these structures, which typically feature molecule-sized cavities, is their ability to function as soluble molecular hosts comprising nanoscale reaction vessels,[5,6] artificial enzymes,[7] or chemical sensors.[8] The compounds have also been employed in the solid state (typically as thin films) where they comprise high-area, high void-volume molecular materials, i.e., materials held together by van der Waals forces.[4] In solid form, they behave as molecular sieves, displaying size cut-offs that correlate with cavity size, or in a few cases, the size of interstitial openings.[4,9,10]

While potentially suitable for many applications, especially those in atmospheric or aqueous environments, the aforementioned molecular materials suffer from instability (solubility) in many organic solvents. Furthermore, they have insufficient mechanical stability to be used as free-standing films or membranes. Additionally, in applications involving vapor or liquid phase separations, comparatively thick films have been required (about 10 μm).[10,11] We reasoned that these limitations could be overcome by appropriately functionalizing squares and then polymerizing them. We further reasoned that by carrying out the polymerization at a liquid–liquid interface—squares in one solvent, linkers in the other—two additional benefits could be gained. First, growth would be self-limiting, thereby facilitating the fabrication of very thin membranes (important for high flux). Second, pinhole defects would be absent because the reactant flux is largest at defect sites, enhancing polymerization at these sites and eliminating the defects.

As shown in Scheme 1, porphyrin-based square assemblies, each functionalized with eight reactive phenol groups, were exposed to either of two bis(acid chloride) molecules (linkers) to generate a nanoporous polyester membrane. Closely related chemistry has previously been used by Wamser et al. to fabricate nonporous, essentially impermeable, films from monomeric porphyrin species.[12] Depending on reaction conditions, thicknesses of harvestable films varied from ~100 nm to 2.5 μm (as measured by tapping mode atomic force microscopy (TMAFM) and profilometry for dried films on glass slides). For a given set of reactant concentrations, the thickness (d) versus reaction time (t) data can be fit well to an exponentially decaying function, $d = \text{constant}\,(1-e^{-kt})$, where a typical value for k is 1×10^{-4} s^{-1}. The self-limiting growth behavior occurs because the polymer itself creates a physical impediment to reactant diffusion and materials growth in the trans-membrane direction.

From TMAFM and profilometry measurements, membrane roughnesses were ca. 10 % for all thicknesses examined. These measurements also occasionally revealed membrane folds or tears, likely created during harvesting (i.e., physical collection, rinsing with acetone, drying in air, Fig. 1a). More extensive tearing, apparently caused by capillary forces, is evident in dried membranes transferred directly from water to air. In-situ AFM phase measurements revealed that, apart from obvious tears, membranes are continuous and appear to feature compositionally homogeneous surfaces (Fig. 1b). Additionally, transmission electron microscopy indicates a non-uniform polymer density; high-density strands are clearly evident on multiple length scales.

The Fourier transform infrared (FT-IR) spectra of the polymers show stretches indicative of both the molecular square sub-unit and the polyester backbone. The presence of the carbonyl stretches from the $Re(CO)_3Cl$ corners, alkyne stretch from the ethynyl spacer, the secondary amine stretch from the amide linkages, and the growth of the ester carbonyl stretch from the polyester backbone are direct evidence of polymer formation based on intact molecular-square subunits. The frequency of the observed C=O stretch from the polyester backbone is in good agreement with those from model compounds.

Visible region spectra of the polymeric membranes are considerably broadened and red-shifted compared to those of

[*] Prof. J. T. Hupp, Dr. M. H. Keefe, J. L. O'Donnell, R. C. Bailey, Prof. S. T. Nguyen
Department of Chemistry and
Center for Nanofabrication and Molecular Self-Assembly
Northwestern University, Evanston, IL 60208–3113 (USA)
E-mail: jthupp@chem.nwu.edu

[**] We thank Prof. John Lindsey for helpful discussions, Prof. Felix Castellano for a sample of $Ru(PNI\text{-}phen)_3^{2+}$ and Prof. Cynthia Larive for PFG-NMR measurements. We thank the U.S. Dept. of Energy, Office of Science, and initially the Northwestern Institute for Environmental Catalysis for financial support. Melinda H. Keefe and Jodi L. O'Donnell have contributed equally to this work.

  DOI: 10.1002/adma.200305353 *Adv. Mater.* **2003**, *15*, No. 22, November 17

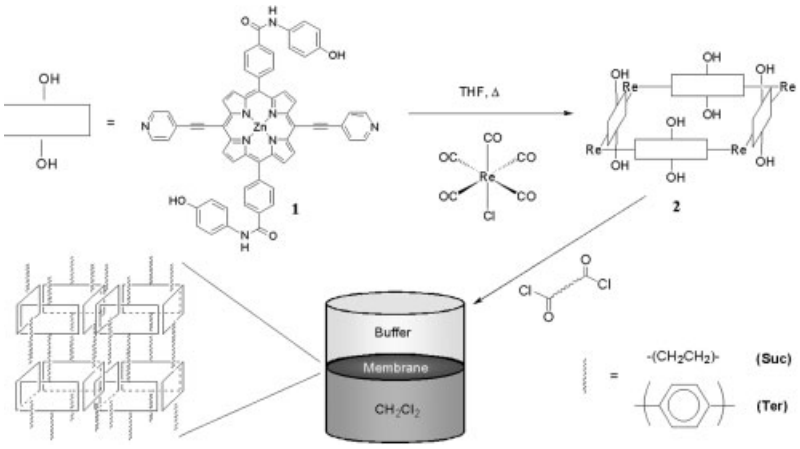

Scheme 1. Synthesis and interfacial polymerization of **2**. For the interfacial polymerization, the square is confined to the aqueous phase and the acid chloride linker to the organic phase. The polymer structure shown is idealized for illustrative purposes; the actual structure lacks net monomer orientation and is almost certainly cross-linked.

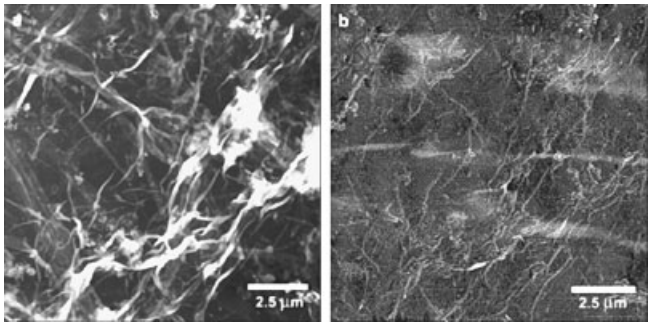

Fig. 1. TMAFM height (a) and phase (b) images in air for a 2/Ter membrane on a glass cover slip. The average membrane thickness was 100 nm.

their constituent monomers, implying significant electronic interaction between porphyrin molecules.[13] Polarized absorption measurements show that the polymerized squares lack a net orientation.

Membrane permeability with respect to a series of redox-active probe molecules was evaluated using slow-sweep (quasi-steady-state) cyclic voltammetry, following placement of the material over a 25 μm diameter platinum microelectrode. Orientation and continuity of the membranes over the electrode was examined visually with a charge-coupled device (CCD) camera (Panasonic KR222, Edmund Scientific). This and other electrochemical approaches take advantage of the fact that current is a measure of molecular flux and that reduction or oxidation of a probe molecule at an electrode creates a concentration gradient in the probe species. Under these conditions transport is well described by a sequential diffusion process: efficient hemispherical diffusion through the low viscosity solvent followed by one-dimensional diffusion through the membrane. The overall flux or current is given by the reciprocal sum of currents for each step in isolation. Under steady-state conditions, this relationship can be used to derive the following:[9]

$$i/i_{\mathrm{mem}} = 1 + 4\,D_s d/\pi r P D_m \qquad (1)$$

where i is the current at a naked electrode, i_{mem} is the current at a membrane-covered electrode, D_s is the probe molecule's diffusion coefficient in solution, D_m is its diffusion coefficient within the membrane, r is the microelectrode radius, and P is the solution-to-film partition coefficient.

As shown in Figure 2, the probe molecule flux increases sharply as the membrane thickness decreases. A reciprocal plot (flux versus 1/d; inset) is linear, consistent with Equation 1. Expressed another way, measured permeabilities (PD_m values) are independent of film thickness, as they should be if membrane diffusion, rather than partitioning, limits the transport. Table 1 summarizes permeability data for five candidate probe molecules.

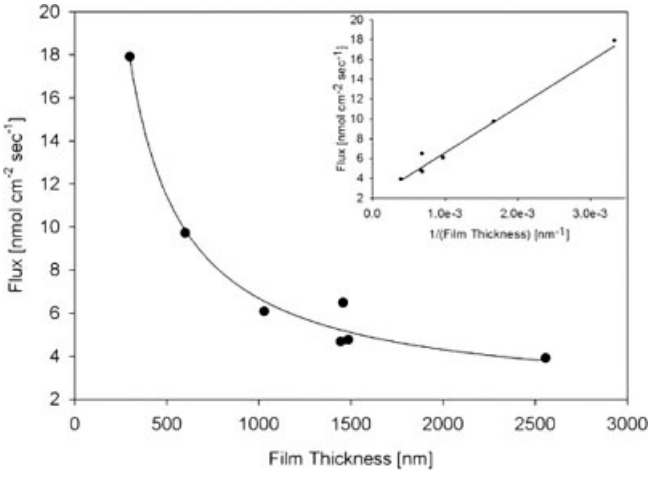

Fig. 2. Probe molecule flux as a function of film thickness for 2/Suc. The line is drawn to show a first order inverse fit to the data. (Inset shows linearity of the reciprocal plot.)

Included for comparison are data for transport through simple molecular films of essentially the same square assembly, {[$Re(CO)_3Cl$]·[5,15-bis(4-ethynylpyridyl)-10,20-bis((4-ethoxycarbonyl)phenyl)Zn(II)porphyrin]}$_4$,[14] and for diffusion through water. Notably, transport through the polymeric squares is 4 to 25 times faster than through the molecular material. The origin of the difference is unclear. But, almost certainly the void volume in a solvent-swollen membrane material is greater than in the corresponding molecular material. The relationship between void volume and transport rate remains to be elucidated for these materials, but it is reasonable to believe that they are related. Transport rates are an essential consideration in many membrane applications, including catalysis, separations, and sensing.

Figure 3, a plot of permeability (PD_m) versus 1/permeant diameter, shows that: a) the transport rate decreases as the probe size increases, and b) beyond a critical size, probe transport is completely blocked. As evidenced by the plot, the

ADVANCED MATERIALS

Table 1. The permeabilities of membrane and thin-films of porphyrinic molecular squares with respect to redox probe molecules of varying size.

Redox probe [a] (Diameter [Å]) [b]	Polymeric film 2/Suc $PD_m \times 10^7$ [cm^2 s^{-1}]	Molecular film [c] $PD_m \times 10^7$ [cm^2 s^{-1}]	Aqueous solution $D_s \times 10^7$ [cm^2 s^{-1}]
FcMeOH (4.5)	13.8 ± 3.5	3.3 ± 0.1	96
$Fe(CN)_6^{4-}$ (6.0)	10.8 ± 2.6	1.95 ± 0.04	71
$Co(phen)_3^{2-}$ (13)	6.3 ± 1.2	0.24 ± 0.01	46
$Fe(bphen(SO_3)_2)_3^{4-}$ (24)	3.4 ± 1.4	very small	12
$Ru(PNI\text{-}phen)_3^{2+}$ [d] (32)	not detected	not measured	not measured

[a] FcMeOH = Ferrocene methanol, phen = 1,10-phenanthroline, bphen$(SO_3)_2$ = 4,7-bis(*p*-sulfonatophenyl)-1,10-phenanthroline, PNI-phen = 5-(*N*-(4-(*N*-piperdidinyl)naphthalene-1,8-dicarboximide.))-1,10-phenanthroline. [b] Radii approximated based upon HyperChem 5.1 geometry optimizations. [c] Data from Zhang et al. [14]. [d] Synthesized by D. S. Tyson, C. R. Luman, X. L. Zhou, F. N. Castellano, *Inorg. Chem.* **2001**, *40*, 4063.

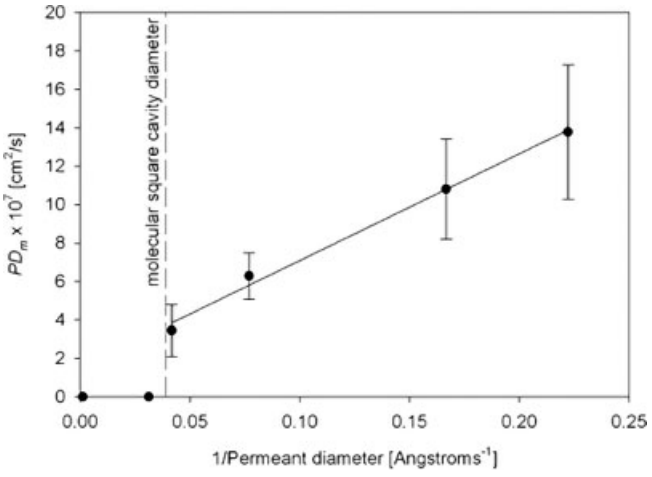

Fig. 3. Dependence of diffusion rate on permeant diameter through 2/Suc. Measurements were made in water as solvent, except for $Ru(PNI\text{-}phen)_3^{2+}$, which was measured in acetonitrile. (Smaller probes were observed to permeate the film from acetonitrile solutions.) The largest probe was a silver nanoparticle. Most measurements were made electrochemically. A few were alternatively or additionally evaluated spectrally by employing the membrane as a porous separator in a U-shaped diffusion cell.

probe cut-off correlates well with the cavity size for an isolated square, strongly suggesting that the cavities define the maximum pore size in the polymer. Below the size cut-off, the observed correlation between PD_m and 1/diameter is reminiscent of the Stokes–Einstein equation for solution-phase diffusion:

$$D = kT/\text{diameter} \times 3\pi\eta \quad (2)$$

If Equation 2 is applicable here, the effective solvent viscosity, η, within the polymer is roughly 7-fold smaller than that in the bulk. This correlation further suggests that the partition coefficient is invariant with permeant molecule composition and charge—a not unreasonable finding given the polymer's charge neutrality and large unit cavity size.

Additional transport and related studies have been carried out successfully in several organic solvents, including tetrahydrofuran (THF) and pyridine (solvents that dissolve the corresponding molecular material). Membrane compatibility with chloroform, acetonitrile, and acetone for extended periods of time (>24 h) has also been demonstrated. Prolonged immersion (several days) in dimethylformamide, however, does eventually degrade the polymer into soluble components. Broad solvent compatibility potentially opens up a number of applications. Also required, of course, is membrane functionality. The copolymerization approach used here is well suited for introduction of functional subunits such as molecular catalysts, the focus of ongoing studies.

In summary, exceptionally thin, porous, polymeric membranes have been generated via self-limiting interfacial copolymerization of reactive molecular-square subunits and difunctional hydrocarbon linkers. The membranes display excellent condensed-phase molecular sieving behavior, with a molecular-size cut-off consistent with expectations based on nanoscale square-cavity-limited permeant transport.

Experimental

The functionalized ligand [5,15-bis(4-ethynylpyridyl)-10,20-bis[4-(*p*-hydroxyamidocarbonyl)phenyl]]zinc(II)porphyrin, **1**, was synthesized via Pd-mediated cross coupling of 4-ethynylpyridine to a dihalogenated porphyrin template [5,15-dibromo-10,20-bis[(4-ethoxycarbonyl)phenyl]]zinc(II)porphyrin, following the methods of Therien and co-workers [15]. Following the hydrolysis of the ethyl ester groups, the resulting carboxylic acid substituents were coupled to 1,4-aminophenol in the presence of standard peptide coupling reagents, benzotriazol-1-yloxytris(dimethylamino)phosphonium hexafluorophosphate (BOP), 1-hydroxybenzotriazole (HOBt), and dimethylaminopyridine (DMAP) [16]. (Coupling of α,ω-dithiol and α,ω-diamino compounds to the carboxylic-acid-containing porphyrin also proved possible, yielding thiol- and amine-derivatized porphyrin ligands [17].) H^1 NMR (400 MHz, DMSO-d_6): δ 10.46 (s, 2H), 9.82 (d, 4H, J = 4.4 Hz), 8.86 (d, 4H, J = 4.4 Hz), 8.84 (d, 4H, J = 5.9 Hz), 8.39 (d, 4H, J = 8.1 Hz), 8.34 (d, 4H, J = 8.1 Hz), 8.1 (d, 4H, J = 5.9 Hz), 7.54 (d, 4H, J = 8.1 Hz), 6.63 (d, 4H, J = 8.1 Hz) ppm. UV-vis (THF): λ_{max} = 448, 650 nm. FTIR (KBr): ν_{O-H} = 3398, $\nu_{C=C}$ = 2189 cm^{-1}. Electron spray mass spectrometry (ESMS): 998.4 (*m/z*, calculated), 998.3 (*m/z*, observed). Elemental Analysis for $C_{60}H_{34}N_8O_4Zn{\cdot}4H_2O$: C, 67.53; H, 3.97; N, 10.51 (calculated), C, 67.59; H, 4.01; N, 10.64 (observed).

By refluxing the hydroxyl functionalized porphyrin with one equivalent of $Re(CO)_5Cl$ in THF for 48 h, the polymerizable molecular square (**2**) was obtained in 95 % yield. Pulsed-field-gradient NMR measurements yielded an effective Stokes diffusion radius consistent with expectations for a square based on a 24 Å × 24 Å metal framework [18,19]. Vapor pressure osmometry measurements (Galbraith Labs) in dimethylformamide (DMF) as solvent yielded a molecular weight of approximately 5275 amu (5216 amu calculated), thereby confirming that the assembly is a square rather than a triangle, pentagon, or other structure. H^1 NMR (400 MHz, DMF-d_7): δ 10.52 (s, 4H), 10.47 (s, 4H), 9.94 (d, 16H), 9.18 (d, 16H), 8.91 (d, 16H), 8.60–8.40 (32H), 8.38 (d, 16H), 7.88 (d, 8H), 7.82 (d, 8H), 6.95 (d, 8H), 6.88 (d, 8H). UV-vis (THF): λ_{max} = 456, 662 nm. FTIR (KBr): $\upsilon_{CO(1)}$ = 2022, $\upsilon_{CO(2)}$ = 1909, $\upsilon_{CO(3)}$ = 1890, $\upsilon_{C=C}$ = 2183, υ_{OH} = 3374, $\upsilon_{NH(1)}$ = 1648, $\upsilon_{NH(2)}$ = 1512 cm^{-1}. Vapor pressure osmometry (DMF): 5275 g mol^{-1} (observed), 5216 g mol^{-1} (calculated). Elemental analysis calculated for $C_{252}H_{144}N_{32}O_{28}Cl_4Zn_4Re_4{\cdot}24H_2O$: C, 53.61; H, 3.43; N, 7.94 (calculated), C, 54.03; H, 3.29; N, 7.65 (observed).

The general procedure for the interfacial polymerization was as follows (Scheme 1): A 100 μM solution of **2**, prepared in a 3:1 pH 11 aqueous carbonate buffer/THF mixture, was layered over a 1 mM solution of linker (1,4-terephthaloyl chloride (Ter) or succinyl chloride (Suc) in CH_2Cl_2). After 3 h, the reactant solutions were removed and the resulting polymer was washed with CH_2Cl_2 and water/THF mixture. The membrane was then harvested and stored over a distilled H_2O reservoir. Reactant concentrations and reaction time were varied to produce membranes of several thicknesses.

Received: May 6, 2003
Final version: July 25, 2003

[1] M. Fujita, *Chem. Soc. Rev.* **1998**, *27*, 417.
[2] P. J. Stang, B. Olenyuk, *Acc. Chem. Res.* **1997**, *30*, 502.
[3] B. J. Holliday, C. A. Mirkin, *Angew. Chem. Int. Ed.* **2001**, *40*, 2022.
[4] P. H. Dinolfo, J. T. Hupp, *Chem. Mater.* **2001**, *13*, 3113.
[5] M. Yoshizawa, Y. Takeyama, T. Kusukawa, M. Fujita, *Angew. Chem. Int. Ed.* **2002**, *41*, 1347.
[6] M. Yoshizawa, Y. Takeyama, T. Okano, M. Fujita, *J. Am. Chem. Soc.* **2003**, *125*, 3243.
[7] M. L. Merlau, M. D. P. Mejia, S. T. Nguyen, J. T. Hupp, *Angew. Chem. Int. Ed.* **2001**, *40*, 4239.
[8] S.-S. Sun, A. J. Lees, *J. Am. Chem. Soc.* **2000**, *122*, 8956.
[9] M. E. Williams, K. D. Benkstein, C. Abel, P. H. Dinolfo, J. T. Hupp, *Proc. Natl. Acad. Sci. USA* **2002**, *99*, 5171.
[10] K. F. Czaplewski, J. T. Hupp, R. Q. Snurr, *Adv. Mater.* **2001**, *13*, 1895.
[11] K. F. Czaplewski, J. Li, J. T. Hupp, R. Q. Snurr, *J. Membr. Sci.* **2003**, *221*, 103.
[12] C. C. Wamser, R. R. Bard, V. Senthilathipan, V. C. Anderson, J. A. Yates, H. K. Lonsdale, G. W. Rayfield, D. T. Friesen, D. A. Lorenz, *J. Am. Chem. Soc.* **1989**, *111*, 8485.
[13] R. B. Beswick, C. W. Pitt, *Chem. Phys. Lett.* **1988**, *143*, 589.
[14] J. Zhang, M. E. Williams, M. H. Keefe, G. A. Morris, S. T. Nguyen, J. T. Hupp, *Electrochem. Solid-State Lett.* **2002**, *5*, E25.
[15] S. M. Lecours, S. G. Dimagno, M. J. Therien, *J. Am. Chem. Soc.* **1996**, *118*, 11 854.
[16] D. Hudson, *J. Org. Chem.* **1988**, *53*, 617.
[17] M. H. Keefe, *Ph.D. Thesis*, Northwestern University **2001**.
[18] W. H. Otto, M. H. Keefe, K. E. Splan, J. T. Hupp, C. K. Larive, *Inorg. Chem.* **2002**, *41*, 6172.
[19] B. Olenyuk, M. D. Levin, J. A. Whiteford, J. E. Shield, P. J. Stang, *J. Am. Chem. Soc.* **1999**, *121*, 10 434.

Planarized Star-Shaped Oligothiophenes as a New Class of Organic Semiconductors for Heterojunction Solar Cells**

By *Rémi de Bettignies*, *Yohann Nicolas*, *Philippe Blanchard*, *Eric Levillain*, *Jean-Michel Nunzi*, and *Jean Roncali**

Photovoltaic (PV) cells based on organic semiconductors are a focus of increasing research effort motivated by the possibility to realize large area, light-weight, and low-cost flexible solar cells, taking advantage of the processability of organic materials.[1–11]

Besides environmental constraints and the predictable exhaustion of fossil energy resources, the strong renewal of interest for organic PV conversion has been boosted by the large improvement in conversion efficiency of organic solar cells accomplished in recent years.[1–11]

It is widely accepted that p–n-like heterojunctions based on adequate combinations of donor (p-type) and acceptor (n-type) molecular or polymeric organic semiconductors represent the most appropriate system to achieve high power conversion efficiencies.[1–3]

[*] Dr. J. Roncali, Y. Nicolas, Dr. P. Blanchard, Dr. E. Levillain
Groupe Systèmes Conjugués Linéaires, IMMO, UMR CNRS 6501
Université d'Angers
2 Bd Lavoisier, F-49045 Angers (France)
E-mail: jean.roncali@univ-angers.fr
Dr. R. de Bettignies, Prof. J.-M. Nunzi
Cellules Photovoltaïques Plastiques, ERT 15
Université d'Angers,
2 Bd Lavoisier, F-49045 Angers (France)

[**] The authors thank TOTAL company for financial support.

Although large area heterojunctions based on interpenetrated networks of donor and acceptor molecules and/or π-conjugated polymers have reached high power conversion efficiencies,[2,4,5] significant progress has also been accomplished in organic PV cells based on vacuum evaporated or laminated multi-layer heterojunctions.[1,3,7,11] Thus, conversion efficiencies exceeding 1 % have been reported for solar cells based on phthalocyanines and acceptors derived from perylene or fullerenes C_{60}.[1,3,7,11]

Whereas thiophene-based π-conjugated oligomers have been widely investigated as organic semiconductors for application in organic field-effect transistors (OFETs),[12] their possible use in solar cells has attracted less attention.[13,14]

It is well known that a vertical orientation of the π-conjugated chains on the surface of the substrate favors high hole mobility in the corresponding OFETs.[12] Conversely, a large absorption of the incident light required for efficient PV conversion implies that the dipole of the chromophore is perpendicular to the direction of the incident light and hence parallel to the surface of the substrate. This problem has been analyzed by Fichou and co-workers, who have shown that alignment of octithiophene molecules parallel to the surface of the substrate produces a substantial improvement in power conversion efficiency of the resulting solar cells.[13]

It is generally accepted that rigid planar structures favor the high exciton mobility needed for large internal conversion quantum yields and high current densities, as illustrated by the high efficiency of solar cells based on phthalocyanines or hexabenzocoronenes.[1,15]

In this context, we report here preliminary results on solar cells based on a new π-conjugated system in which three linear oligothiophene (nTs) chains are connected to a central planar and rigid trithienobenzene core (**1**) (see Scheme 1). Using *N*,*N*′-bistridecylperylenedicarboxyimide (**3**) as the acceptor and electron-transport layer, we have carried out a comparative analysis of the spectral response and power efficiency of two series of heterojunction solar cells in which compound **1** and the linear reference compound **2** have been used as donor and hole-transport materials.

The synthesis of compounds **1** and **2** will be published elsewhere. These compounds melt at 160 and 135 °C, respectively, and can thus be easily processed by vacuum sublimation without degradation. In fact, thermogravimetry shows that compound **1** begins to degrade only above 430 °C.

Figure 1 shows the electronic absorption spectra of compounds **1** and **2** in methylene chloride solution and as thin solid films sublimed on glass.

Comparison of the solution spectra of compounds **1** and **2** shows that the absorption maximum (λ_{max}) shifts bathochromically from 379 nm (3.27 eV) for the linear compound **2** to 405 nm (3.06 eV) for the star-shaped compound **1**. This red shift shows that the combined effects of planarization and rigidification of the central core leads to a significant enhancement of π-electron delocalization associated with a decrease of the highest occupied–lowest unoccupied molecular orbital (HOMO–LUMO) gap. This conclusion is further supported

 DOI: 10.1002/adma.200305168